Journal of Molecular Spectroscopy 251 (2008) 305–313

Contents lists available at ScienceDirect

Journal of Molecular Spectroscopy

journal homepage: www.elsevier.com/locate/jms

Torsion–rotation global analysis of the first three torsional states (v_t = 0, 1, 2) and terahertz database for methanol

Li-Hong Xu [a,*], J. Fisher [a], R.M. Lees [a], H.Y. Shi [a], J.T. Hougen [b], J.C. Pearson [c], B.J. Drouin [c], G.A. Blake [d], R. Braakman [d]

[a] Centre for Laser, Atomic, and Molecular Sciences (CLAMS), Department of Physics, University of New Brunswick, PO Box 5050, Saint John, NB, Canada E2L 4L5
[b] Optical Technology Division, National Institute of Standards and Technology, Gaithersburg, MD 20899-8441, USA
[c] Jet Propulsion Laboratory, California Institute of Technology, Pasadena, CA 91109, USA
[d] Department of Chemistry & Chemical Engineering, California Institute of Technology, Pasadena, CA 91109, USA

ARTICLE INFO

Article history:
Received 5 February 2008
In revised form 11 March 2008
Available online 30 March 2008

Keywords:
Large amplitude internal rotational motion
Microwave
Millimeter wave
Terahertz
Global modeling
Fourier transform

ABSTRACT

Stimulated by recent THz measurements of the methanol spectrum in one of our laboratories, undertaken in support of NASA programs related to the Herschel Space Observatory (HSO) and the Atacama Large Millimeter Array (ALMA), we have carried out a global analysis of available microwave and high-resolution infrared data for the first three torsional states (v_t = 0, 1, 2), and for J values up to 30. This global fit of approximately 5600 frequency measurements and 19000 Fourier transform far infrared (FTFIR) wavenumber measurements to 119 parameters reaches the estimated experimental measurement accuracy for the FTFIR transitions, and about twice the estimated experimental measurement accuracy for the microwave, submillimeter-wave, and terahertz transitions. The present fit is essentially a continuation of our earlier work, but we have greatly expanded our previous data set and have added a large number of new torsion–rotation interaction terms to the Hamiltonian in our previously used computer program. The results, together with a number of calculated (but unmeasured) transitions, including their line strength, estimated uncertainty, and lower state energy, are made available in the supplementary material as a database formatted to be useful for astronomical searches. Some discussion of several open spectroscopic problems, e.g., (i) an improved notation for the numerous parameters in the torsion–rotation Hamiltonian, (ii) possible causes of the failure to fit frequency measurements to the estimated measurement uncertainty, and (iii) pitfalls to be avoided when intercomparing apparently identical parameters from the internal axis method and the rho axis method are also given.

1. Introduction

There are a large number of fits of methanol torsion–rotation transitions in the literature of the last two decades [1–22], which differ in rotational and torsional quantum number coverage, in the model Hamiltonian and computer program used, and in the precision obtained in the fit. Refs. [1–8] are associated in one way or another with the laboratory at the University of New Brunswick in Canada, while Refs. [9–22] are representative torsion–rotation fits from other laboratories. The present global fit of the first three torsional states (v_t = 0, 1, 2) of methanol up to J = 30 is essentially a continuation of our earlier global fits of the torsional ground state (v_t = 0, $J \leqslant 20$) by itself [1] and of the first two torsional states (v_t = 0, 1, $J \leqslant 20$) together [2]. A global fit similar to the present one has been completed for $CH_3{}^{18}OH$ [8], but the available microwave (MW) and millimeter-wave (MMW) data set for that isotopolog is much smaller than the data set treated here.

The present fit was stimulated by recent Jet Propulsion Laboratory (JPL) THz measurements, carried out with a new spectrometer [23] based on a number of THz technologies developed for the heterodyne instrument for the far infrared (HIFI), which is scheduled to be flown on the Herschel Space Observatory (HSO) in 2008, and for the Atacama Large Millimeter Array (ALMA). Central to the design of both instruments was the development of fixed tuned broadband frequency multipliers, and moderate to high-power broadband amplifiers which have sufficient spectral purity for laboratory spectroscopy.

Because of the historical lack of good THz sources and detectors, this region is relatively unexplored, but with imminent HIFI/Herschel access to this new and vast region of interstellar emission and absorption, it is critical to characterize known target molecules as fully as possible. In particular, methanol and its isotopologs, because of their intrinsically strong spectra, contribute significantly

* Corresponding author. Fax: +1 506 648 5948.
E-mail address: lxu@unbsj.ca (L.-H. Xu).

0022-2852/$ - see front matter © 2008 Elsevier Inc. All rights reserved.
doi:10.1016/j.jms.2008.03.017

to the "grass" in any interstellar radio astronomy spectrum, and the need for a line list permitting removal of this grass during searches for new molecules led to methanol being one of the first test molecules on the new JPL instrument. The latter test covers almost the entire region from 330 to 1830 GHz, greatly extending the available data set and necessitating a corresponding extension of the global fitting and modeling. Measurement uncertainty depends on the frequency region and is estimated to be ±50 kHz for $\nu < 750$ GHz, ±100 kHz for 750 GHz $< \nu <$ 1.655 THz, and ±200 kHz for $\nu >$ 1.655 THz. More than 15 000 methanol lines have been detected using the JPL submillimeter analysis program (SMAP) [24].

The A and E components of the $v_t = 2$ torsional level lie near 480 and 640 cm^{-1}, respectively, as measured from the bottom of the potential well. These two levels are well above the top of the barrier at $V_3 = 374$ cm^{-1}, but they are still well below the lowest small-amplitude vibration v_8 near 1034 cm^{-1} (with A and E components near 1162 and 1171 cm^{-1}, respectively, when measured from the bottom of the torsional well [25]). Thus, it should in principle be possible to fit torsion–rotation states of the first three torsional levels using the same torsion–rotation Hamiltonian as was used previously [1–8]. Nevertheless, new difficulties arise, since an increase in torsional excitation leads to more level crossings and perturbations, as well as to a denser spectrum with more line overlap and more anomalous intensity variation within branches (compared to that expected for a rigid molecule). For example, as shown in Fig. 1 of [2], torsion-K-rotation splittings for $v_t = 2$ can reach values greater than 150 cm^{-1}. Since we wish to fit the new JPL THz transitions to a precision of 50 kHz or so, the more important torsion–rotation interactions must be described by the Hamiltonian and treated by the fitting program to a precision of about 1 part in 10^8.

Nearly 25 000 transitions are included in the present fit. Some 5600 of these are frequency measurements, meaning that line centers were determined from spectra typically obtained with precision tunable microwave, submillimeter, or THz sources. The remaining 19 000 lines were obtained from high-resolution Fourier transform infrared spectrometers. With a data set of this size, it is not feasible to determine appropriate measurement uncertainties for individual lines, nor to critically evaluate duplicate wavenumber or frequency measurements in the literature to determine the best value for an individual line. We therefore decided to view our present fit in the spirit of a "living document" subject to future updates and improvements. In this respect, we encourage measurement laboratories represented in the data set to assess carefully how we have treated their data, and to partition (if appropriate) their measurements into an optimum set (for which they specify their highest measurement precision) and a less good set (for which they specify a reduced measurement precision). In addition, when measurements presently in the fit are known (or thought) to be inferior to those in a "better" line list, we ask that this be brought to our attention. Extending the quantum number coverage of the present data set would represent a new undertaking. We are, however, interested in refining our current fit by using new or improved measurements to fill in gaps within our present quantum number coverage, i.e., within $0 \leqslant v_t \leqslant 2$ and $J \leqslant 30$.

2. Data set

The data set consists of more than 19 000 far infrared (FIR) wavenumber measurements and 5600 microwave (MW), submillimeter-wave, and terahertz (THz) frequency measurements. The FIR transitions were taken with only minor changes from the same RITZ-program analysis of the Fourier transform spectra used in our earlier fits [26]. The present extension of quantum number coverage allows us to bring about 65% of the RITZ assigned and compiled transitions into the fit (with the remainder being transitions to the $v_t = 3$ and 4 torsional levels and at wavenumbers above 950 cm^{-1} to v_8 small-amplitude vibrational level plus a few transitions to v_7 and v_5 small-amplitude vibrational levels). Many older MW measurements in the range covered by the Toyama atlas (7–200 GHz) [27] were replaced by the newer measurements in that atlas. The first few columns of Table 1 give an overview of the numbers and types of measurements included in the fit, together with some indication of their assigned experimental uncertainties. Table 1 does not specify the laboratory (or database) of origin of a measurement, but this can be found in the computer output files deposited as Supplementary Data (see Appendix A), where lines are tagged by an early attempt at such documentation.

When carrying out a global fit on a large and diverse data set, a principal difficulty associated with the data set itself is the assignment of reliable measurement uncertainties. This is also true for the present case, as for example the new JPL measurements were

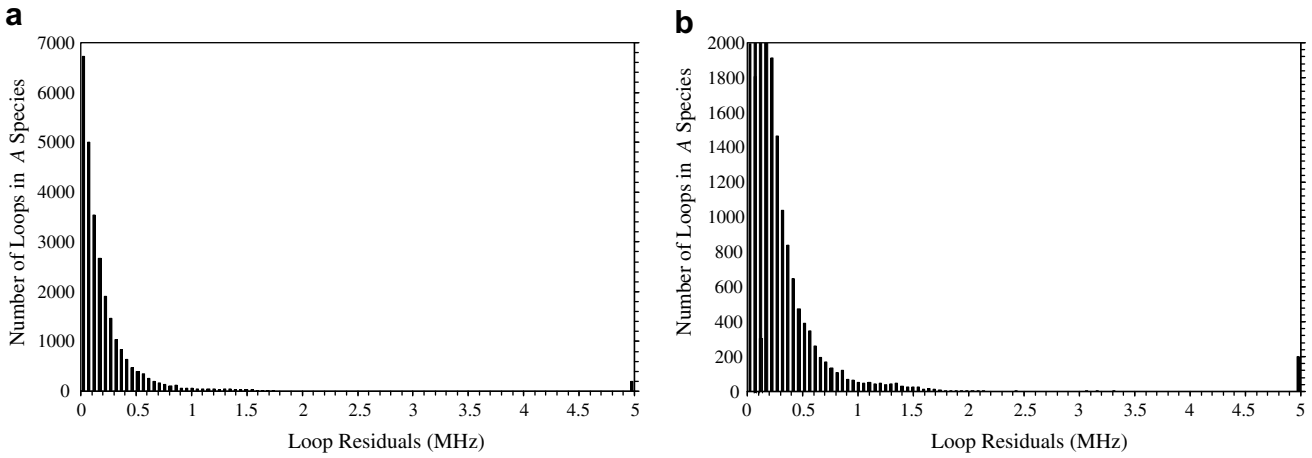

Fig. 1. (a) The total number of closed loop sums with $N = 3$, 4, 5, and 6 lines for frequency measured transitions between levels of A species in our data set, as a function of their deviation from zero. The bar at 5 MHz represents all loop sums $\geqslant$5 MHz. (b) An expanded version of the same figure, where only numbers of residuals above 0.2 MHz fall on scale. If the measurement uncertainty $\Delta\nu_{meas}$ is the same for all lines in a loop, then 68% of the loop sums should be less than $\Delta\nu_{meas}\sqrt{N}$, which takes the value of 100 kHz for a loop of four lines with measurement precision of 50 kHz. Clearly, the very long tail of loop sums above 0.2 MHz present a problem when their lines are included in a least-squares fit with assigned uncertainties of 50 kHz. Since these loops involve no calculated frequencies, one must conclude that the long tail arises either from larger than expected measurement uncertainties and/or from spectral misassignments.

Table 1
Statistics of the data set for the torsion–rotation global fit[a] to $v_t = 0, 1, 2$ torsional states of CH_3OH

MW[b]	RMS[c]		No. of data[d]	FTFIR[b]	Uncertainties[e]		RMS[c]		No. of data[d]
	Unitless	MHz			cm^{-1}	MHz	Unitless	cm^{-1}	
All MW lines	1.91	0.195	5667	All FTFIR lines			1.28	0.00031	19055
$v_t = 0 \leftarrow 0$	1.59	0.141	2974	$v_t = 0 \leftarrow 0$	0.0002	6	1.27	0.00030	2828
$v_t = 1 \leftarrow 0$	2.23	0.381	67	$v_t = 1 \leftarrow 0$	0.0002	6	1.53	0.00031	6768
$v_t = 1 \leftarrow 1$	1.95	0.184	1830	$v_t = 2 \leftarrow 0$	0.0002	6	1.25	0.00025	2615
$v_t = 2 \leftarrow 1$	2.78	0.556	79	$v_t = 1 \leftarrow 1$	0.00035	10.5	1.07	0.00037	2485
$v_t = 2 \leftarrow 2$	2.71	0.287	717	$v_t = 2 \leftarrow 1$	0.00035	10.5	0.92	0.00032	3448
				$v_t = 2 \leftarrow 2$	0.00035	10.5	0.94	0.00033	911
Uncertainty[e] in MHz									
0.050		0.098	2737		0.0002			0.00029	11384[f]
0.070		0.091	431		0.00035			0.00034	7671[f]
0.080		0.087	108						
0.100		0.229	1286						
0.200		0.319	1012						
1.000		0.380	93						

[a] The overall unitless standard deviation for this fit of 24722 data to 119 parameters is 1.45.
[b] The microwave (MW) and Fourier transform far infrared (FTFIR) transitions are grouped first by torsional quantum number v_t, and then by their assigned uncertainties in the fit. Weights used for all lines in the fit are $1/(\text{uncertainty})^2$.
[c] Weighted (unitless) and unweighted (in MHz or cm^{-1}) root-mean-square residuals from the global fit.
[d] The number of transitions in each category included in the least squares fit.
[e] Measurement uncertainties assigned to the various types of transitions (type B, $k = 1$ [28]).
[f] The measurement uncertainties of 827 lines with $v''_t = 0$ were increased to 0.00035 cm^{-1} due to overlaps, unresolved splittings, etc.

carried out in six different regions using different multipliers. Extensive inter-laboratory comparisons are not generally possible in the THz region, but Fig. 2 in a recent paper by the Bologna group [29] indicates that disagreements as large as 150 kHz between present state-of-the-art measurements of the same line in different laboratories can occur for transitions near 1 THz.

For this reason, we checked a large number of sums over closed combination-difference-loops of $N = 3, 4, 5$, or 6 transitions, based on the present assignments for those transitions. For lines of equal measurement uncertainty $\Delta\nu_{meas}$, one would expect the loops to sum to zero to within $\Delta\nu_{meas}\sqrt{N}$. Figs. 1 and 2 give example histograms of these results. The significant tail above 200 kHz in each histogram indicates that occasional lines have unsuspected measurement errors much greater than 100 kHz, though it is certainly not clear at the moment what fraction of the sums in this tail arise from misassignments and what fraction from measurement errors. Transitions that did not satisfy loop-sum relations or were multiply assigned were excluded from the fit. As mentioned in the introduction, one of the goals associated with the "living document" designation of our present fit is to seek the help of the spectroscopic community in gradually locating and correcting these unsuspected mismeasurements and/or misassignments.

For simplicity, the uncertainties of all MW and millimeter-wave (MMW) lines were taken as ±50 kHz in the fit, except for a few unresolved *K*-doublet transitions which were given uncertainties of ±100 to ±200 kHz. The uncertainties of the FIR transitions from the Fourier transform spectra were grouped according to lower torsional state energies, and were set to ±6 MHz (0.0002 cm^{-1}) for $v_t = 0 \leftarrow 0$, $1 \leftarrow 0$, and $2 \leftarrow 0$ transitions, and to ±10.5 MHz (0.00035 cm^{-1}) for $v_t = 1 \leftarrow 1$, $2 \leftarrow 1$, and $2 \leftarrow 2$ transitions. In certain cases we increased the uncertainties of FIR lines known to be strongly overlapped, or of transitions expected to be very weak because the rotational quantum numbers *J* and *K* change in the opposite direction.

3. Computer program changes

The computer program used in our earlier fits was originally obtained from I. Kleiner [30], who now has a version available on the web [31]. The general approach involves transferring

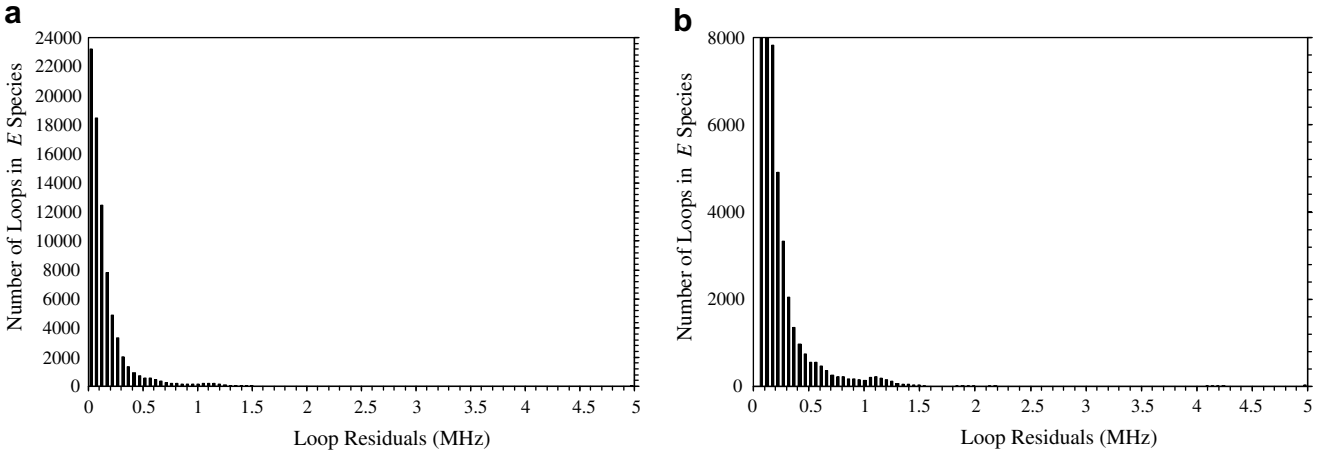

Fig. 2. (a) The total number of closed loop sums with $N = 3, 4, 5$, and 6 lines for frequency measured transitions between levels of *E* species in our data set, as a function of their deviation from zero. The bar at 5 MHz represents all loop sums $\geqslant 5$ MHz. (b) An expanded version of the same figure, where only numbers of residuals above 0.2 MHz fall on scale. See the caption to Fig. 1 for additional comments.

the large amplitude internal rotation motion from the vibrational part of the Hamiltonian to the rotational part, yielding a four-dimensional zeroth-order Hamiltonian of the form

$$H = F(P_\gamma + \rho P_a)^2 + (1/2)V_3(1-\cos 3\gamma) + AP_a^2 + BP_b^2 + CP_c^2 + D_{ab}(P_aP_b + P_bP_a), \quad (1)$$

where γ is the internal rotation angle, P_γ is its conjugate momentum, and P_a, P_b, P_c are the rotational angular momentum operators. Higher-order terms are generated via the traditional power series approach by taking products of integer powers of the momenta, $P_\gamma^p P_a^q P_b^r P_c^s$, with terms $(1-\cos 3t\gamma)$ in the Fourier expansion of the internal rotation potential function, and then using group theory and time reversal to eliminate symmetry-forbidden terms. A total order [15] $n \equiv l + m$ is assigned to each term, where the torsional order $l \equiv p + 2t$ and the rotational order $m \equiv q + r + s$. The basis set consists of products of symmetric-top rotational functions $|KJM\rangle$ and torsional exponential functions $e^{+iu\gamma}/\sqrt{2\pi}$, where u is an integer. Diagonalization of the Hamiltonian in this basis set is performed in two steps [9]. The first torsion-K-rotation step contains the low-order terms not involving P_b and P_c. The second step then retains about 1/3 of the lower energy eigenfunctions from the first step and uses this truncated basis set to set up the full torsion–rotation Hamiltonian matrix involving all terms.

We have modified the program in some ways useful for the present fits, but the general approach has not been changed. First, subroutines for matrix diagonalization and matrix inversion, which were previously included in the code, have been replaced by LAPACK routines [32,33], which are now almost universally available and also well documented (with respect to rounding, precision, etc.). Some increase in speed was also achieved, since LAPACK is almost always optimized for whichever system it is implemented on. Second, all of the previously hard-coded dimensions have been replaced with a few predefined constants, so that increasing dimensions (as required when going to higher J, for example) now requires little more than a recompile. Third, a substantial number of new parameters (i.e., new higher-order terms in the Hamiltonian) were added to the program. These were checked mainly by requiring the eigenvalues of an algebraically determined H^2 to be the square of the eigenvalues of a Hamiltonian H containing lower-order terms appropriately chosen to generate the desired higher-order terms in H^2. During this process, we systematically re-examined all parameters and their corresponding operators in Table 2 to ensure mutual consistency, particularly for parameters multiplying operators involving anti-commutators. One inconsistency was indeed detected, for the $F_{Kbc}(c_8)$ term, as indicated in a footnote to Table 2. Finally, some effort was put into making sure that the program compiled and ran as expected on several different systems. (It is currently known to work with GNU g77, Portland Group Fortran, and Compaq Fortran compilers.)

The addition of new parameters required a corresponding nomenclature. It is common (though unwritten) knowledge that the naming conventions used in much of the internal rotation literature border on the chaotic, and indeed the names in the program for many parameters we have added respect this tradition (see column 3 of Table 2). With 119 parameters in our fit, however, we were led to think about some non-traditional naming scheme with more mnemonic value. The main principle of our presently favored scheme is to agree on a letter for a low-order term, and then add one or more of the six subscripts m, J, K, ab, bc, and ac to indicate higher-order corrections to these terms. The m, J, and K subscripts have proved convenient for symmetric-top internal rotor molecules [34,35], and we have simply added the ab, bc, and ac subscripts to allow for terms occurring in asymmetric-top internal rotor molecules.

Starting the procedure with the $\{nlm\} = \{220\}$ (in the notation and ordering scheme of Ref. [15], where m unfortunately has a different meaning from the subscript m of Refs. [34,35], as explained in a footnote to Table 2) torsional parameters F and V_3, which multiply P_γ^2 and $(1-\cos 3\gamma)/2$, respectively, leads to new names for one of the {440} parameters and eight of the {422} parameters, as shown in the fourth column of Table 2. (Names previously used in the literature are given in parentheses following the name proposed here.) Even though the coefficient of $P_\gamma P_a$ is $-2F\rho$ rather than ρ, we decided to represent higher-order corrections to $P_\gamma P_a$ by the symbol ρ with subscripts chosen from the six listed above. This gives new names for the {431} and {413} parameters, again as shown in column four of Table 2. This process is then continued for the $n \geqslant 6$ terms in the table.

3.1. Relationship of RAM and previous IAM parameters

An additional complication arises in the literature because the torsional angular momentum in the internal axis system (IAM) differs from that in the rho axis system (RAM) [36]. Both of these rather widely used axis systems have their a axis along the ρ vector (i.e., neither is a principal axis system) and the c axis perpendicular to the COH plane, but the IAM axis system involves an additional rotation about the a axis to cancel out the angular momentum associated with the internal rotation. Because of this difference, it turns out that the IAM torsional momentum operator P_γ^{IAM} corresponds to [9,36] the RAM operator $(P_\gamma^{\mathrm{RAM}} + \rho P_a)$. This leads to a large difference between reported constants that on the surface appear equivalent in the Hamiltonian. Thus, for example, when comparing IAM and RAM values for the distortion constant Δ_K that is nominally the coefficient of P_a^4, one must also account for contributions from the P_γ^4, $P_\gamma^3 P_a$, $P_\gamma^2 P_a^2$, and $P_\gamma P_a^3$ terms. The equations which relate the RAM parameters of this and earlier papers in the series with the IAM parameters of Herbst et al. [9] (written in terms of the traditional coefficients k_4, k_3, k_2, k_1, rather than in terms of their new names F_m, ρ_m, F_K, ρ_K proposed in Table 2) are as follows:

$$\begin{aligned}
\Delta_K^{\mathrm{RAM}} &= \Delta_K^{\mathrm{IAM}} - \rho k_1^{\mathrm{IAM}} - \rho^2 k_2^{\mathrm{IAM}} - \rho^3 k_3^{\mathrm{IAM}} - \rho^4 k_4^{\mathrm{IAM}} \\
k_1^{\mathrm{RAM}} &= k_1^{\mathrm{IAM}} + 2\rho k_2^{\mathrm{IAM}} + 3\rho^2 k_3^{\mathrm{IAM}} + 4\rho^3 k_4^{\mathrm{IAM}} \\
k_2^{\mathrm{RAM}} &= k_2^{\mathrm{IAM}} + 3\rho k_3^{\mathrm{IAM}} + 6\rho^2 k_4^{\mathrm{IAM}} \\
k_3^{\mathrm{RAM}} &= k_3^{\mathrm{IAM}} + 4\rho k_4^{\mathrm{IAM}} \\
k_4^{\mathrm{RAM}} &= k_4^{\mathrm{IAM}}
\end{aligned} \quad (2)$$

We can invert these relations to obtain the IAM parameters in terms of the RAM parameters:

$$\begin{aligned}
\Delta_K^{\mathrm{IAM}} &= \Delta_K^{\mathrm{RAM}} + \rho k_1^{\mathrm{RAM}} - \rho^2 k_2^{\mathrm{RAM}} + \rho^3 k_3^{\mathrm{RAM}} - \rho^4 k_4^{\mathrm{RAM}} \\
k_1^{\mathrm{IAM}} &= k_1^{\mathrm{RAM}} - 2\rho k_2^{\mathrm{RAM}} + 3\rho^2 k_3^{\mathrm{RAM}} - 4\rho^3 k_4^{\mathrm{RAM}} \\
k_2^{\mathrm{IAM}} &= k_2^{\mathrm{RAM}} - 3\rho k_3^{\mathrm{RAM}} + 6\rho^2 k_4^{\mathrm{RAM}} \\
k_3^{\mathrm{IAM}} &= k_3^{\mathrm{RAM}} - 4\rho k_4^{\mathrm{RAM}} \\
k_4^{\mathrm{IAM}} &= k_4^{\mathrm{RAM}}
\end{aligned} \quad (3)$$

As an example of the dramatic difference in magnitude, the value of Δ_K^{RAM} derived from Table 2 is 255.5 MHz, whereas the value of Δ_K^{IAM} obtained from the above relation using the other parameter values in the table is 1.67 MHz, as shown in Table 3, in reasonable agreement with the 1.27 MHz reported previously by Lees and Baker [37]. Thus, it is essential when intercomparing parameters from different models and fits to be very clear about the precise definitions of the terms in the Hamiltonian and to be sure to transform them appropriately.

4. Fitting results

Table 1 summarizes the quality of the fit for various categories of data. It can be seen that the 19000 FTFIR lines are fitted to between 1 and 1.5 times their estimated measurement uncertainties,

Table 2
The 119 torsion–rotation parameters (in cm^{-1}) in the global fit of v_t = 0, 1, and 2 torsional states of CH_3OH methanol and comparison with a previous fit of v_t = 0, 1 torsional states

Term order {*nlm*}[a]	Operator[b]	Parameter[b]		v_t = 0, 1, and 2[d] (present work)	v_t = 0, 1[d] (Ref. [2])
		In program	Literature[c]		
{220}	P_γ^2	FPARA	F	27.64684641(28)	27.64682(2)
	$(1-\cos 3\gamma)/2$	V3	V_3	373.554746(12)	373.594(7)
{211}	$P_\gamma P_a$	RHORHO	ρ[e]	0.8102062230(37)[e]	0.81020601(1)[e]
{202}	P_a^2	OA	A	4.2537233(71)	4.253724(2)
	P_b^2	B	B	0.8236523(70)	0.8235767(2)
	P_c^2	C	C	0.7925575(71)	0.7925390(3)
	$\{P_a,P_b\}$	DAB	D_{ab}	−0.0038095(38)	−0.004171(4)
{440}	P_γ^4	AK4	F_m (k_4)	$-8.976763(48)\times10^{-3}$	$-8.985(1)\times10^{-3}$
	$(1-\cos 6\gamma)/2$	V6	V_6	−1.319650(85)	−1.60(5)
{431}	$P_\gamma^3 P_a$	AK3	ρ_m (k_3)	$-3.504714(14)\times10^{-2}$	$-3.5072(3)\times10^{-2}$
{422}	$P_\gamma^2 P^2$	GV	F_J (G_v)	$-1.373(31)\times10^{-4}$	$-1.18853(4)\times10^{-4}$
	$P_\gamma^2 P_a^2$	AK2	F_K (k_2)	$-5.188031(18)\times10^{-2}$	$-5.1906(4)\times10^{-2}$
	$P_\gamma^2\{P_a,P_b\}$	DELTA	F_{ab} (Δ_{ab})	$3.112(23)\times10^{-3}$	$1.9(1)\times10^{-4}$
	$2P_\gamma^2(P_b^2-P_c^2)$	C1	F_{bc} (c_1)	$-0.1955(97)\times10^{-4}$	$-1.43(1)\times10^{-4}$
	$(1-\cos 3\gamma)P^2$	FV	V_{3J} (F_v)	$-2.4324(69)\times10^{-3}$	$-2.38796(8)\times10^{-3}$
	$(1-\cos 3\gamma)P_a^2$	AK5	V_{3K} (k_5)	$1.117844(23)\times10^{-2}$	$1.1183(1)\times10^{-2}$
	$(1-\cos 3\gamma)\{P_a,P_b\}$	ODAB	V_{3ab} (d_{ab})	$9.07791(65)\times10^{-3}$	$9.048(2)\times10^{-3}$
	$(1-\cos 3\gamma)(P_b^2-P_c^2)$	C2	V_{3bc} (c_2)	$-8.698(21)\times10^{-5}$	$-7.60(3)\times10^{-5}$
	$\sin 3\gamma\{P_a,P_c\}$	DAC	D_{3ac} (D_{ac})	$5.177(29)\times10^{-2}$	$1.52(1)\times10^{-2}$
	$\sin 3\gamma\{P_b,P_c\}$	DBC	D_{3bc} (D_{bc})	$0.538(12)\times10^{-3}$	$-1.02(1)\times10^{-3}$
{413}	$P_\gamma P_a P^2$	ALV	ρ_J (L_v)	$-2.305(54)\times10^{-4}$	$-1.90289(9)\times10^{-4}$
	$P_\gamma P_a^3$	AK1	ρ_K (k_1)	$-3.4254(13)\times10^{-2}$	$-3.459(1)\times10^{-2}$
	$P_\gamma(P_a^2P_b+P_bP_a^2)$	ODELTA	ρ_{ab} (δ_{ab})	$4.496(33)\times10^{-3}$	$6.6(2)\times10^{-4}$
	$P_\gamma\{P_a,(P_b^2-P_c^2)\}$	C4	ρ_{bc} (c_4)	$-0.7047(94)\times10^{-4}$	$-1.91(1)\times10^{-4}$
{404}	$-P^4$	DJ	Δ_J	$1.688465(31)\times10^{-6}$	$1.68627(5)\times10^{-6}$
	$-P^2P_a^2$	DJK	Δ_{JK}	$9.20(25)\times10^{-5}$	$8.480(2)\times10^{-5}$
	$-P_a^4$	DK	Δ_K	$8.524(10)\times10^{-3}$	$8.77(1)\times10^{-3}$
	$-2P^2(P_b^2-P_c^2)$	ODELN	δ_J	$5.9414(33)\times10^{-8}$	$5.873(2)\times10^{-8}$
	$-\{P_a^2,(P_b^2-P_c^2)\}$	ODELK	δ_K	$5.7361(89)\times10^{-5}$	$5.241(7)\times10^{-5}$
	$\{P_a,P_b\}P^2$	DABJ	D_{abJ}	$-0.548(23)\times10^{-7}$	$1.26(6)\times10^{-7}$
	$\{P_a^3,P_b\}$	DABK	D_{abK}	$1.443(11)\times10^{-3}$	$4.6(1)\times10^{-4}$
{660}	P_γ^6	AK4B	F_{mm} (k_{4B})	$1.01639(75)\times10^{-5}$	$1.044(2)\times10^{-5}$
	$(1-\cos 9\gamma)/2$	V9	V_9	−0.05126(34)	1.0(2)
{651}	$P_\gamma^5 P_a$	AK3B	ρ_{mm} (k_{3B})	$6.7042(35)\times10^{-5}$	$6.931(7)\times10^{-5}$
{642}	$P_\gamma^4 P^2$	AMV	F_{mJ} (M_v)	$9.215(14)\times10^{-8}$	$8.63(8)\times10^{-8}$
	$P_\gamma^4 P_a^2$	BK1	F_{mK} (K_1)	$1.79670(69)\times10^{-4}$	$1.863(1)\times10^{-4}$
	$P_\gamma^4\{P_a,P_b\}$	DELTAB	F_{mab} ($\Delta\Delta_{ab}$)	$0.773(54)\times10^{-6}$	2.544×10^{-10} (fixed)
	$2P_\gamma^4(P_b^2-P_c^2)$	C3	F_{mbc} (c_3)	$0.214(18)\times10^{-7}$	
	$\{(1-\cos 3\gamma),P_\gamma^2\}P^2$	AK7J	V_{3mJ} (k_{7J})	$9.4(16)\times10^{-6}$	
	$(1-\cos 6\gamma)P^2$	ANV	V_{6J} (N_v)	$2.64(53)\times10^{-5}$	$-4.4(3)\times10^{-6}$
	$(1-\cos 6\gamma)P_a^2$	BK2	V_{6K} (K_2)	$-1.3905(25)\times10^{-4}$	$-1.89(4)\times10^{-4}$
	$(1-\cos 6\gamma)\{P_a,P_b\}$	ODAB6	V_{6ab} (dd_{ab})	$-0.388(16)\times10^{-4}$	$1.55(5)\times10^{-4}$
	$(1-\cos 6\gamma)(P_b^2-P_c^2)$	C11	V_{6bc} (c_{11})	$-3.3840(70)\times10^{-5}$	$-6.7(3)\times10^{-6}$
	$\sin 6\gamma\{P_a,P_c\}$	DAC6	D_{6ac}	$3.401(58)\times10^{-4}$	
{633}	$P_\gamma^3 P_a P^2$	AK3J	ρ_{mJ} (k_{3J})	$7.875(69)\times10^{-7}$	$3.30(2)\times10^{-7}$
	$P_\gamma^3 P_a^3$	AK3K	ρ_{mK} (k_{3K})	$2.51512(70)\times10^{-4}$	$2.6183(9)\times10^{-4}$
	$P_\gamma^3\{P_a^2,P_b\}$	ODELTB	ρ_{mab} ($\delta\delta_{ab}$)	$1.61(11)\times10^{-6}$	-8.790×10^{-10} (fixed)
	$P_\gamma^3\{P_a,(P_b^2-P_c^2)\}$	C12	ρ_{mbc} (c_{12})	$6.903(52)\times10^{-7}$	$-2.1(8)\times10^{-9}$
	$\{(1-\cos 3\gamma),P_aP^2P_\gamma\}$	AK6J	ρ_{3J} (k_{6J})	$2.11(27)\times10^{-5}$	
	$\{(1-\cos 3\gamma),P_a^3P_\gamma\}$	AK6K	ρ_{3K} (k_{6K})	$0.385(63)\times10^{-4}$	$2.02(6)\times10^{-4}$
{624}	$P_\gamma^2P^4$	GVJ	F_{JJ} (g_v)	$0.5243(22)\times10^{-9}$	$1.13(1)\times10^{-9}$
	$P_\gamma^2P_a^2P^2$	AK2J	F_{JK} (k_{2J})	$1.769(19)\times10^{-6}$	$4.93(2)\times10^{-7}$
	$P_\gamma^2\{P_a,P_b\}P^2$	DELTAJ	F_{Jab}	$2.75(21)\times10^{-9}$	
	$2P_\gamma^2P^2(P_b^2-P_c^2)$	C1J	F_{Jbc} (c_5)		-5.776×10^{-13} (fixed)
	$P_\gamma^2P_a^4$	AK2K	F_{KK} (k_{2K})	$1.94907(47)\times10^{-4}$	$2.0411(3)\times10^{-4}$
	$P_\gamma^2\{P_a^3,P_b\}$	DELTAK	F_{Kab}	$8.29(59)\times10^{-7}$	
	$P_\gamma^2\{P_a^2,(P_b^2-P_c^2)\}$[f]	C1K	F_{Kbc} (c_8)	$1.518(15)\times10^{-6}$	$2[-0.15(38)\times10^{-9}]$[f]
	$(1-\cos 3\gamma)P^4$	OFV	V_{3JJ} (f_v)	$9.149(21)\times10^{-9}$	$6.27(7)\times10^{-9}$
	$(1-\cos 3\gamma)P_a^2P^2$	AK5J	V_{3JK} (k_{5J})	$7.6(26)\times10^{-6}$	$-5.3(2)\times10^{-7}$
	$(1-\cos 3\gamma)\{P_a,P_b\}P^2$	ODABJ	V_{3Jab} (d_{abJ})	$-2.027(17)\times10^{-7}$	
	$2(1-\cos 3\gamma)(P_b^2-P_c^2)P^2$	C2J	V_{3Jbc} (c_{2J})	$1.251(43)\times10^{-9}$	
	$(1-\cos 3\gamma)P_a^4$	AK5K	V_{3KK} (f_k)	$0.78(10)\times10^{-4}$	$3.3(1)\times10^{-4}$
	$(1-\cos 3\gamma)\{P_a^3,P_b\}$	ODABK	V_{3Kab} (d_{abK})	$-1.538(79)\times10^{-7}$	
	$(1-\cos 3\gamma)\{P_a^2,(P_b^2-P_c^2)\}$	C2K	V_{3Kbc} (c_9)	$7.232(86)\times10^{-6}$	-1.201×10^{-8} (fixed)
	$\sin 3\gamma P^2\{P_a,P_c\}$	DACJ	D_{3acJ}	$-2.888(23)\times10^{-7}$	
	$\sin 3\gamma P^2\{P_b,P_c\}$	DBCJ	D_{3bcJ}	$-1.070(58)\times10^{-8}$	
	$\sin 3\gamma\{P_a^3,P_c\}$	DACK	D_{3acK}	$0.70(10)\times10^{-6}$	
	$\sin 3\gamma\{P_a^2,\{P_b,P_c\}\}$	DBCK	D_{3bcK}	$-0.585(70)\times10^{-6}$	
{615}	$P_\gamma P_a P^4$	OLV	ρ_{JJ} (l_v)	$0.8961(62)\times10^{-9}$	$1.34(1)\times10^{-9}$
	$P_\gamma P_a^3P^2$	AK1J	ρ_{JK} (λ_v)	$1.231(14)\times10^{-6}$	$3.51(2)\times10^{-7}$
	$P_\gamma P^2\{P_a^2,P_b\}$	DAGJ	ρ_{Jab}	$1.91(18)\times10^{-9}$	
	$P_\gamma P^2\{P_a,(P_b^2-P_c^2)\}$	C4J	ρ_{Jbc} (c_7)	$0.426(33)\times10^{-9}$	6.997×10^{-11} (fixed)
	$P_\gamma P_a^5$	AK1K	ρ_{KK} (l_k)	$7.9805(24)\times10^{-5}$	8.396×10^{-5} (fixed)
	$P_\gamma\{P_a^3,(P_b^2-P_c^2)\}$	C4K	ρ_{Kbc} (c_{7K})	$1.119(16)\times10^{-6}$	

(*continued on next page*)

Table 2 (*continued*)

Term order {*nlm*}[a]	Operator[b]	Parameter[b]		v_t = 0, 1, and 2[d] (present work)	v_t = 0, 1[d] (Ref. [2])
		In program	Literature[c]		
{606}	P^6	HJ	H_J	$-1.191(16)\times10^{-12}$	-1.446×10^{-12} (fixed)
	$P^4P_a^2$	HJK	H_{JK}	$4.781(40)\times10^{-10}$	$4.53(6)\times10^{-10}$
	$P_a^4P^2$	HKJ	H_{KJ}	$2.336(37)\times10^{-7}$	$1.03(1)\times10^{-7}$
	P_a^6	HK	H_K	$1.35675(51)\times10^{-5}$	$1.4264(2)\times10^{-5}$
	$P^2\{P_a^2,(P_b^2-P_c^2)\}$	OHJK	h_{JK}	$0.427(31)\times10^{-9}$	8.757×10^{-11} (fixed)
	$\{P_a^4,(P_b^2-P_c^2)\}$	OHK	h_K	$2.928(54)\times10^{-7}$	
{880}	P_γ^8	AK4C	F_{mmm} (k_{4BB})	$-0.5887(30)\times10^{-7}$	
{871}	$P_\gamma^7P_a$	AK3C	ρ_{mmm} (k_{3BB})	$-0.3447(19)\times10^{-6}$	
{862}	$P_\gamma^6P^2$	AK4BJ	F_{mmJ}	$-0.4129(60)\times10^{-9}$	
	$P_\gamma^6P_a^2$	AK4BK	F_{mmK}	$-0.8527(55)\times10^{-6}$	
	$(1-\cos9\gamma)P^2$	V9J	V_{9J}	$-1.31(66)\times10^{-6}$	
	$(1-\cos9\gamma)\{P_a,P_b\}$	ODAB9	V_{9ab}	$-0.819(43)\times10^{-4}$	
{853}	$P_\gamma^5P_aP^2$	AK3BJ	ρ_{mmJ}	$-1.635(26)\times10^{-9}$	
	$P_\gamma^5P_a^3$	AK3BK	ρ_{mmK}	$-1.1548(88)\times10^{-6}$	
{844}	$P_\gamma^4P_a^2P^2$	G4J2K2	F_{mJK} (K_{1J})	$-2.097(63)\times10^{-9}$	
	$P_\gamma^4P^2\{P_a,P_b\}$	DG4J	F_{mJab}	$-8.67(73)\times10^{-12}$	
	$P_\gamma^4P_a^4$	G4K4	F_{mKK} (K_{1K})	$-0.9220(84)\times10^{-6}$	
	$P_\gamma^4\{P_a^2,(P_b^2-P_c^2)\}$	G4BCK	F_{mKbc}	$0.886(95)\times10^{-10}$	
	$(1-\cos6\gamma)P^4$	C6J4	V_{6JJ} (N_{vJ})	$4.44(32)\times10^{-10}$	
	$(1-\cos6\gamma)P^2P_a^2$	C6J2K2	V_{6JK}	$1.953(61)\times10^{-7}$	
	$(1-\cos6\gamma)P^2\{P_a,P_b\}$	CABJ	V_{6Jab}	$3.50(15)\times10^{-8}$	
	$2(1-\cos6\gamma)P^2(P_b^2-P_c^2)$	C6BCJ	V_{6Jbc}	$1.326(52)\times10^{-9}$	
	$(1-\cos6\gamma)P_a^4$	C6K4	V_{6KK}	$-3.143(66)\times10^{-7}$	
	$(1-\cos6\gamma)\{P_a^3,P_b\}$	CABK	V_{6Kab} (dd_{abK})	$2.26(21)\times10^{-7}$	
	$(1-\cos6\gamma)\{P_a^2,(P_b^2-P_c^2)\}$	C6BCK	V_{6Kbc} (c_{11K})	$-1.351(43)\times10^{-7}$	
{835}	$P_\gamma^3P_a^3P^2$	GAJ2K2	ρ_{mJK}	$-1.062(64)\times10^{-9}$	
	$P_\gamma^3P_a^5$	GAK4	ρ_{mKK}	$-4.305(48)\times10^{-7}$	
	$P_\gamma^3\{P_a^3,(P_b^2-P_c^2)\}$	AG3BCK	ρ_{mKbc}	$8.66(94)\times10^{-11}$	
	$\{(1-\cos3\gamma),P_a^3P_\gamma\}P^2$	AK6JK	ρ_{3JK}	$5.58(22)\times10^{-8}$	
{826}	$P_\gamma^2P_a^2P^4$	GJ4K2	F_{JJK}	$1.477(32)\times10^{-12}$	
	$P_\gamma^2P_a^4P^2$	GJ2K4	F_{JKK}	$-1.90(20)\times10^{-10}$	
	$P_\gamma^2P^2\{P_a^3,P_b\}$	DELTJK	F_{JKab}	$4.53(59)\times10^{-12}$	
	$P_\gamma^2P_a^6$	GK6	F_{KKK}	$-1.068(15)\times10^{-7}$	
	$P_\gamma^2\{P_a^5,P_b\}$	DELTKK	F_{KKab}	$-0.89(11)\times10^{-11}$	
	$(1-\cos3\gamma)P^2P_a^4$	FJ2K4	V_{3JKK}	$0.914(36)\times10^{-7}$	
	$(1-\cos3\gamma)P_a^6$	FK6	V_{3KKK}	$-1.00(46)\times10^{-10}$	
	$\sin3\gamma P^4\{P_a,P_c\}$	DACJJ	D_{3acJJ}	$-0.717(46)\times10^{-11}$	
	$\sin3\gamma P^2\{P_a^3,P_c\}$	DACJK	D_{3acJK}	$-1.593(30)\times10^{-9}$	
{817}	$P_\gamma P_a^3P^4$	AGJ4K2	ρ_{JJK}	$1.192(20)\times10^{-12}$	
	$P_\gamma P_a^7$	AGK6	ρ_{KKK} (1_{KK})	$-1.033(21)\times10^{-8}$	
{10 10 0}	P_γ^{10}	AK4D	F_{mmmm}	$-0.940(20)\times10^{-10}$	
{10 9 1}	$P_\gamma^9P_a$	AK3D	ρ_{mmmm}	$-4.663(92)\times10^{-10}$	
{10 8 2}	$P_\gamma^8P_a^2$	AK4CK	F_{mmmK}	$-0.939(17)\times10^{-9}$	
{10 7 3}	$P_\gamma^7P_a^3$	AK3CK	ρ_{mmmK}	$-0.957(17)\times10^{-9}$	
{10 6 4}	$P_\gamma^6P_a^4$	AK4BK4	F_{mmKK}	$-4.915(82)\times10^{-10}$	
{10 5 5}	$P_\gamma^5P_a^5$	AK3BK4	ρ_{mmKK}	$-1.017(16)\times10^{-10}$	

[a] Order of the Hamiltonian term in the notation of Ref. [15]: $n = l + m$, where n is the total order of the operator, l is the order of the torsional factor, and m is the order of the rotational factor. Note that the rotational-order m of Ref. [15], used in the first column of this table, does not have the same meaning as the subscript m of Refs. [34,35], used in the fourth column of this table.

[b] $\{A, B\} \equiv AB + BA$. The product of the parameter and operator from a given row yields the term actually used in the torsion–rotation Hamiltonian of the fitting program, except for F, ρ, and A, which occur in the Hamiltonian in the form $F(P_\gamma + \rho P_a)^2 + AP_a^2$.

[c] The first name given in this column is the one used in this manuscript. The name in parentheses can be found in the literature.

[d] Parameter uncertainties are given in parentheses, and represent one standard deviation in the last digit (type A, $k = 1$, [28]).

[e] ρ is unitless, but all subscripted versions of ρ (e.g., ρ_m, ρ_J, ρ_K, etc.) are in cm^{-1}.

[f] A factor of 2 in the operator multiplying c_8 in Table 2 of Ref. [2] was removed in the present program, so the numerical value of c_8 from Ref. [2] must be multiplied by 2 in the present table.

where we have assigned all infrared transitions coming from the $v_t = 0$ state a measurement uncertainty of 0.00020 cm^{-1}, and all hot-band lines an uncertainty of 0.00035 cm^{-1}. We consider this quite acceptable, and will not comment on the lines measured in wavenumber units further in this paper.

The 5600 lines measured in frequency units are fit to between 1 and 2.8 times their estimated measurement uncertainties, which is somewhat worse than for the FTFIR lines. In particular, the 2700 lines thought to be measured to 50 kHz actually only fit to 100 kHz, and the 1300 lines thought to be measured to 100 kHz only fit to 230 kHz. As usual, the question arises as to whether these large residuals arise from model error or from measurement error, and significant further effort will be required to resolve this issue. In this connection, the procedure for assigning measurement uncertainties (i.e., the procedure for critically evaluating the frequency measurements) must itself be revisited, as discussed under the several different subheadings below. A principal reason that we decided to opt for a "living document" approach was the hope that some of these large residuals in the frequency measurements can be reduced through future theoretical and experimental effort.

Lines from the 1995 Toyama atlas. These measurements [27] lie in the range 7 GHz $\leqslant \nu \leqslant$ 200 GHz, and are divided into three groups in the atlas, with estimated measurement accuracies of 10, 30, or 50 kHz. Older measurements which exhibited large observed-minus-calculated residuals in our earlier fits have been partially replaced by lines from this atlas (and assigned a

Table 3
Conversion of {*n*} = {4} torsional and *K*-rotational parameters from RAM values to IAM values

{*nlm*}	Parameter name (current ≡ previous)	Operator	RAM value[a] (cm^{-1})	RAM[a] (MHz)	IAM[b] (MHz)	L&B[c] (MHz)
{440}	$F_m \equiv k_4$	P_γ^4	−0.008976763(48)	−269.12	−269.12	−249
{431}	$\rho_m \equiv k_3$	$P_\gamma^3 P_a$	−0.03504714(14)	−1050.69	−178.53	−132
{422}	$F_K \equiv k_2$	$P_\gamma^2 P_a^2$	−0.05188031(18)	−1555.33	−61.46	−79.7
{413}	$\rho_K \equiv k_1$	$P_\gamma P_a^3$	−0.034254(13)	−1026.91	−3.23	−3.5
{404}	Δ_K	$-P_a^4$	+0.008524(10)	+255.54	+1.67	+1.27

[a] RAM parameter values in cm^{-1} and MHz from Table 2 of the present work.
[b] IAM parameter values calculated from Eqs. (3), with $\rho = 0.810206223$.
[c] IAM parameter values from Ref. [37].

measurement uncertainty of 50 kHz), since in almost all cases lines from the atlas were within 50 kHz of the values predicted in these fits. This good agreement suggests that it might be appropriate, if the one and two hundred kHz residuals of the preceding paragraph turn out not to arise from model error, to explore fits in which all lines in the 7–200 GHz region in our data set are replaced by lines from the Toyama atlas together with their smaller measurement uncertainties of 10 and 30 kHz when indicated.

Tuneable far infrared (TuFIR) lines. TuFIR measurements, which range from below 1 THz to above 6 THz [16,38], were included in our earlier works [1,2] but caused a great deal of trouble. It was originally believed, based on the rule-of-thumb that a line center can be measured to a precision approximately equal to its half width divided by its signal to noise ratio (*S*/*N*), that many of these lines should be given measurement uncertainties less than 50 kHz. Later estimates based on combination-difference-loop histograms similar to those shown in Figs. 1 and 2, however, indicated that a more realistic measurement precision was closer to 150 or 200 kHz [39]. The cause for this is not yet established, but one possibility might be the presence of unknown weak transitions (grass) lying under some of the strong lines in molecules like CH_3OH that act to perturb the line shape and thereby prevent a correct determination of the line center to the theoretical limit of (linewidth)/(*S*/*N*), when (*S*/*N*) > 1000.

Köln lines. These measurements [14,40] range from 0.8 GHz to 1.2 THz, and most of the new measurements in Ref. [40] have stated measurement uncertainties much smaller than the value of 50 kHz assigned in our present fit. Just as with the Toyama data, some of the trends of residuals for these lines suggest that new fits using the smaller reported uncertainties should be explored.

JPL lines. Many of these lines deviate from their calculated values in the fit by significantly more than 100 kHz. While some of these discrepancies, which frequently involve v_t, *J*, or *K* values at the limits of the quantum numbers included in our data set, are clearly the result of inadequacies in the model, others, as suggested by the long tails in histograms like those shown in Figs. 1 and 2, may well involve unsuspected blending and/or other measurement problems. Misassignments, while certainly possible, cannot be the whole problem, since many residuals are within the linewidths of the transitions involved.

K-type doublets. For many values of K_a, the series of transition doublets to the pairs of levels with quantum numbers $J_{K_aJ-K_a}$ and $J_{K_aJ-K_a+1}$ start out at $J = K_a$ as single sharp features and then gradually broaden and split as *J* increases. This leads to the systematic occurrence of unresolved broad blends in the spectrum. In principle, in a very sophisticated least-squares fit one should fit the contour of a blended pair, but in practice one often fits only to the center of the blended feature (since the individual intensities are generally nearly equal). In our present fits, we resorted to the latter less sophisticated expedient of fitting two calculated transitions to the same measured line, while assigning the line measurement an uncertainty comparable to the calculated splitting. While it would be desirable to upgrade this procedure for improved fits in the future, it is not an unreasonable approach since in many cases the measured frequency of the blended line does fall very close to halfway between the two calculated frequencies of the doublet components.

5. Methanol THz data base

In support of the Orion molecular line surveys [41] for the upcoming Herschel [42], ALMA [43], and SOFIA [44] missions, there is a need for a comprehensive line list including information such as transition quantum numbers, lower state energy, and transition strength, and one of the outputs of the present work is just such a list. Since extrapolation beyond the quantum number coverage of any given measurement data set rapidly becomes unreliable, we have chosen a torsional state limit of $v_t \leqslant 2$ (no extrapolation) and rotational limits of $J \leqslant 35$ (an extrapolation of 5 units beyond the fitted data set) and $K \leqslant 15$ (little or no extrapolation, depending on v_t). These quantum number limits correspond to torsion-*K*-rotation energies [2] up to 1400 cm^{-1}, well above the ~370 cm^{-1} torsional potential barrier height, and give a wide coverage of observable transitions with strong to medium line strength.

Along with the calculated transition frequencies, uncertainty estimates were also determined for each transition from the variance–covariance matrix of the least-squares analysis as described in reference [45]. Lower state energies are given, referenced to the $K = 0$ A $v_t = 0$ level about 127 cm^{-1} above the bottom of the torsional potential well, as was done in reference [46].

For a transition $J'_{v'_t,K'_a,\sigma} \leftarrow J''_{v''_t,K''_a,\sigma}$ of σ torsional symmetry, the total torsion–rotational line strength is calculated as:

$$|\langle v'_t, J', K'_a, \sigma | \alpha_{Za}\mu_a + \alpha_{Zb}\mu_b | v''_t, J'', K''_a, \sigma \rangle|^2, \tag{4}$$

where α is the direction cosine matrix, and the dipole moment components μ_a and μ_b should in principle be represented by Fourier expansions in $\cos 3n\gamma$, but are in fact represented here by their first (constant) term. There is some variation in the literature concerning the values of the permanent dipole moment components of methanol and their dependence on rotational and torsional states [46]. The line strengths in the present line list have been calculated using values $\mu_a = 0.899$ D and $\mu_b = -1.44$ D [46] (1 D ≅ 3.3356 × 10^{-30} C m). A more systematic study of methanol line intensities in the far infrared region is currently underway [47].

The line list containing the data set in the present work along with the calculated lower state energies, transition line strengths and estimated uncertainties is available as Supplementary Data (see Appendix A).

6. Discussion

The principal conclusions and principal remaining problems in this work are illustrated by the tables and figures. The overview in Table 1 shows that approximately 5600 frequency measure-

ments and 19000 wavenumber measurements have been fitted to 119 parameters, and that the wavenumber measurements are fit to their estimated experimental accuracy, while the frequency measurements are fit to between 2 and 3 times their estimated experimental accuracy. The histograms of A and E species loop defects in Figs. 1 and 2 indicate that further progress in fitting the frequency measurements cannot be expected until the long tail of loop defects above 0.2 MHz is eliminated by remeasurement of the offending lines.

Comparison of the presently determined molecular fitting parameters with those from our previous work [2] in Table 2 indicates that most of the low-order parameters, with $\{n\} = \{2\}$ or $\{4\}$, show excellent stability when considered in terms of percent changes, and quite good stability when considered in terms of agreement within several of their standard uncertainties. This indicates that the approximate doubling of the data set and parameter set sizes in this work has not led to any fundamental changes in spectroscopic interpretation. The larger changes in parameters with $n \geqslant 6$, are not surprising, since the previous fit had no parameters with $n \geqslant 8$. We believe that these parameters and the associated program code give very reliable calculated values, as presented in the Supplementary Data, for positions (with calculated uncertainties) and intensities of unmeasured lines characterized by quantum numbers representing interpolation within the $0 \leqslant v_t \leqslant 2$ and $0 \leqslant J \leqslant 30$ range of our fitted data, and reasonably reliable values for transitions with $31 \leqslant J \leqslant 35$, which represent a relatively small extrapolation outside our fitted range. We also believe that the "new" notation suggested in Table 2 for various torsion–rotation parameters in methanol represents a mnemonically appealing improvement over the old.

Table 3 suggests a possible direction for future investigation, i.e., whenever two "equivalent" forms of a Hamiltonian are available, the general question arises of whether one form is better than the other. In the present case, this question takes the form of whether the RAM or IAM parameters in equations analogous to Eqs. (2) and (3) are better, in the sense of needing fewer adjustable parameters (from the very high-order sets) to obtain the same quality of fit. In addition to an intuitive preference for a minimum number of adjustable parameters in the model Hamiltonian, the fitting instabilities arising from parameter correlation in fits with a very large number of parameters would presumably be significantly reduced when the most efficient set of parameters is used. When all five of the RAM terms on the left of Eq. (2) are adjusted in the fit, the final residuals and overall standard deviation of the fit should be the same as when all five of the IAM terms on the left of Eqs. (3) are adjusted. The question in this paragraph makes sense, however, when less than five of the terms in either set are adjusted, since then differences in the residuals and standard deviation will arise. A similar remark holds for equivalent RAM and IAM sets of other higher-order terms.

It is interesting to make a preliminary observation from Table 3, which shows for the set of five parameters considered in Eqs. (2) and (3), and for the fit of the $v_t = 0$, 1, and 2 torsional states of methanol carried out here, that a theoretically very appealing monotonic decrease in magnitude as one goes from the pure torsional limit $\{nlm\} = \{440\}$ to the pure rotational limit $\{nlm\} = \{404\}$ is obtained for the IAM parameters, but not for the RAM parameters. It seems likely, however, that the optimum choice between IAM and RAM parameters will be more complicated, i.e., that the most efficient set of parameters will depend on the size of the internal rotational splittings compared to the rotational spacings, on the energies of the torsional states included in the fit compared to the barrier height, and on the degree of asymmetry and rigidity of the molecule, so that any systematic investigation of the most efficient set of parameters would require a significant amount of programming and pair-wise fitting comparisons.

Acknowledgments

The authors thank Drs. I. Kleiner and M. Godefroid for making their acetaldehyde (CH_3CHO) internal rotation global fitting program available for this work. L.H.X. and R.M.L. thank the Natural Sciences and Engineering Research Council of Canada for financial support of this research program. J. Fisher is grateful for NSERC-USRA (Undergraduate Summer Research Award) support. Portions of the research described in this paper were carried out at the Jet Propulsion Laboratory, California Institute of Technology, under a contract with the National Aeronautics and Space Administration.

Appendix A. Supplementary data

Supplementary data for this article are available on ScienceDirect (www.sciencedirect.com) and as part of the Ohio State University Molecular Spectroscopy Archives (http://library.osu.edu/sites/msa/jmsa_hp.htm). Supplementary data associated with this article can be found, in the online version, at doi:10.1016/j.jms.2008.03.017.

References

[1] Li-Hong Xu, J.T. Hougen, J. Mol. Spectrosc. 169 (1995) 396–409.
[2] Li-Hong Xu, J.T. Hougen, J. Mol. Spectrosc. 173 (1995) 540–551.
[3] Li-Hong Xu, M.S. Walsh, R.M. Lees, J. Mol. Spectrosc. 179 (1996) 269–281.
[4] M.S. Walsh, Li-Hong Xu, R.M. Lees, J. Mol. Spectrosc. 188 (1998) 85–93.
[5] M.S. Walsh, Li-Hong Xu, R.M. Lees, I. Mukhopadhyay, G. Moruzzi, B.P. Winnewisser, S. Albert, R.A.H. Butler, F.C. DeLucia, J. Mol. Spectrosc. 204 (2000) 60–71.
[6] L.-H. Xu, H.S.P. Müller, F.F.S. van der Tak, S. Thorwirth, J. Mol. Spectrosc. 228 (2004) 220–229.
[7] H.S.P. Müller, Li-Hong Xu, Floris van der Tak, J. Mol. Struct. 795 (2006) 114–133.
[8] J. Fisher, G. Paciga, Li-Hong Xu, S.B. Zhao, G. Moruzzi, R.M. Lees, J. Mol. Spectrosc. 245 (2007) 7–20.
[9] E. Herbst, J.K. Messer, F.C. DeLucia, P. Helminger, J. Mol. Spectrosc. 108 (1984) 42–57.
[10] T. Anderson, E. Herbst, F.C. DeLucia, Astrophys. J. Suppl. 64 (1987) 703–714.
[11] T. Anderson, F.C. DeLucia, E. Herbst, Astrophys. J. Suppl. 72 (1990) 797–814.
[12] T. Anderson, E. Herbst, F.C. DeLucia, Astrophys. J. Suppl. 74 (1990) 647–664.
[13] T. Anderson, E. Herbst, F.C. DeLucia, Astrophys. J. Suppl. 82 (1992) 405–444.
[14] S.P. Belov, G. Winnewisser, E. Herbst, J. Mol. Spectrosc. 174 (1995) 253–269.
[15] K. Nakagawa, S. Tsunekawa, T. Kojima, J. Mol. Spectrosc. 126 (1987) 329–340.
[16] H. Odashima, F. Matsushima, K. Nagai, S. Tsunekawa, K. Takagi, J. Mol. Spectrosc. 173 (1995) 404–422.
[17] Y.-B. Duan, L. Wang, K. Takagi, J. Mol. Spectrosc. 193 (1999) 418–433.
[18] Y.-B. Duan, L. Wang, X.T. Wu, I. Mukhopadhyay, K. Takagi, J. Chem. Phys. 111 (1999) 2385–2391.
[19] Y.-B. Duan, A.B. McCoy, L. Wang, K. Takagi, J. Chem. Phys. 112 (2000) 212–219.
[20] L. Wang, Y.-B. Duan, F. Matsushima, K. Takagi, Chem. Phys. Lett. 365 (2002) 432–439.
[21] O.I. Baskakov, M.A.O. Pashaev, J. Mol. Spectrosc. 151 (1992) 282–291.
[22] M.A. Mekhtiev, P.D. Godfrey, J. Mol. Spectrosc. 180 (1996) 54–71.
[23] B.J. Drouin, F.W. Maiwald, J.C. Pearson, Rev. Sci. Instrum. 76 (2005) 093113.
[24] Available from: <http://spec.jpl.nasa.gov/ftp/pub/calpgm/SMAP/>.
[25] Li-Hong Xu, R.M. Lees, P. Wang, L.R. Brown, I. Kleiner, J.W.C. Johns, J. Mol. Spectrosc. 228 (2004) 453–470.
[26] G. Moruzzi, B.P. Winnewisser, M. Winnewisser, I. Mukhopadhyay, F. Strumia, Microwave, Infrared and Laser Transitions of Methanol—Atlas of Assigned Lines from 0 to 1258 cm^{-1}, CRC, ISBN 0-8493-2478-5, 1995.
[27] S. Tsunekawa, T. Ukai, A. Toyama, K. Takagi, Microwave Frequencies of the CH_3OH Molecule in the Frequency Range from 7 to 200 GHz, Toyama University Japan, private communication.
[28] B.N. Taylor, C.E. Kuyatt, Guidelines for Evaluating and Expressing the Uncertainty of NIST Measurement Results, NIST Technical Note 1297, 1994. Available from: <http://physics.nist.gov/cuu/Uncertainty/index.html>.
[29] F. Tinti, L. Bizzocchi, C. Degli Esposti, L. Dore, ApJ 669 (2007) L113–L116.
[30] I. Kleiner, private communication.
[31] BELGI at <http://info.ifpan.edu.pl/~kisiel/prospe.htm#introt>.
[32] Available from: <http://www.netlib.org/lapack/>.
[33] Certain commercial or internet-available products are identified in this paper in order to specify adequately the experimental or theoretical procedures. In no case does such identification imply recommendation or endorsement by the National Institute of Standards and Technology, nor does it imply that the products are necessarily the best available for the purpose.

[34] M. Wong, I. Ozier, W.L. Meerts, J. Mol. Spectrosc. 102 (1983) 89–111.
[35] J. Schroderus, N. Moazzen-Ahmadi, I. Ozier, J. Chem. Phys. 115 (2001) 1392–1404.
[36] J.T. Hougen, I. Kleiner, M. Godefroid, J. Mol. Spectrosc. 163 (1994) 559–586.
[37] R.M. Lees, J.G. Baker, J. Chem. Phys. 48 (1968) 5299–5318.
[38] F. Matsushima, K.M. Evenson, L.R. Zink, J. Mol. Spectrosc. 164 (1994) 517–530.
[39] F. Matsushima, private communication.
[40] H.S.P. Müller, K.M. Menten, H. Mäder, Astron. Astrophys. 428 (2004) 1019–1026.
[41] P. Schilke, D.J. Benford, T.R. Hunter, D.C. Lis, T.G. Phillips, ApJ Suppl. 132 (2001) 281–364.
[42] Available from: <http://herschel.esac.esa.int/>.
[43] Available from: <http://www.alma.nrao.edu/>.
[44] Available from: <http://www.sofia.usra.edu/>.
[45] W.H. Kirchhoff, J. Mol. Spectrosc. 41 (1972) 333–380.
[46] Li-Hong Xu, F.J. Lovas, J. Phys. Chem. Ref. Data 26 (1997) 17–156. and references therein.
[47] Linda R. Brown, John C. Pearson, private communication.